https://doi.org/10.5194/egusphere-2025-1233
Preprint. Discussion started: 26 March 2025


# Molecular level Insights on the Photosensitized Chemistry of Nonanoic Acid in the Presence of 4-Benzoylbenzoic Acid at the Sea Surface Microlayer

**Ahmed Abdelmonem[1,*], Dana Glikman[2], Yiwei Gong[1], Björn Braunschweig[2], Harald Saathoff[1], Johannes Lützenkirchen[3], and Mohammed H. Fawey[4]**

*1. Institute of Meteorology and Climate Research, Karlsruhe Institute of Technology (KIT), 76344 Eggenstein-Leopoldshafen, Germany*

*2. Institute of Physical Chemistry and Center for Soft Nanoscience, University of Münster, 48149 Münster, Germany*

*3. Institute of Nuclear Wastes Disposal, Karlsruhe Institute of Technology (KIT), 76344 Eggenstein-Leopoldshafen, Germany*

*4. Physics Department, Faculty of Science, Sohag University, 82524 Sohag, Egypt.*

**** Corresponding Author: ahmed.abdelmonem@kit.edu***

https://doi.org/10.5194/egusphere-2025-1233
Preprint. Discussion started: 26 March 2025



## Abstract

Atmospheric chemistry and aerosol-water interactions significantly impact Earth's climate by influencing the energy budget. Organic compounds concentrated at air-water interfaces, such as the sea-surface microlayer (SML), are key contributors to atmospheric aerosols and undergo complex photochemical reactions. This study combines sum-frequency generation (SFG) spectroscopy and mass spectrometry (MS) to investigate the photochemical interactions of nonanoic acid (NA) and 4-benzoylbenzoic acid (4-BBA) at the air-water interface under varying solar spectra, pH, and salinity conditions. SFG spectroscopy detected aromatic signals at the interface, unreported in prior studies using bulk techniques, highlighting the partitioning of non-surface-active compounds to the organic surface layer. The study demonstrates that 4-BBA acts both as a photosensitizer and a photoproduct precursor, with its photolysis being more active under shorter UV wavelengths. Reaction mechanisms were found to depend on solar spectrum, pH, and salinity, with salinity accelerating photoreaction rates by increasing surface concentrations of 4-BBA. These findings emphasize the need to account for environmental variables such as light intensity, geographic location, and atmospheric conditions when modeling photochemical processes. The results provide insights into surface-bulk photochemical coupling and their implications for aerosol formation across diverse natural water systems, from oceans to cloud droplets.


**Keywords: Sum-frequency generation (SFG) spectroscopy; Mass spectrometry; Air-water interface; Sea surface microlayer; Aerosol formation; volatile organic compounds.**

https://doi.org/10.5194/egusphere-2025-1233
Preprint. Discussion started: 26 March 2025


## 1. Introduction

The Earth's climate system is impacted by atmospheric chemistry and aerosol-water interactions, which affect the energy budget through scattering of sunlight and absorption of thermal radiation (Meerkötter and Vázquez-Navarro, 2012). Atmospheric aerosols have both natural and human-made sources which vary depending on the location, time of year, and meteorological conditions (Boucher, 2015). Sources include natural sources (e.g. dust, sea spray, volcanic ash, wildfires, and biological particles), anthropogenic sources (e.g. industrial and agricultural processes, transportation, and energy production), secondary formation (e.g. through chemical reactions between pollutants in the atmosphere), and waste disposal (e.g. landfills, open burning) (Ouafo-Leumbe et al., 2018). It has been estimated that volatile organic compounds (VOCs) can make up a significant fraction of atmospheric aerosols, particularly in urban and industrial areas. It has been shown that up to 91.9 TgC per year of organic vapors could be emitted from the oceans into the marine atmosphere and have a potential contribution to organic aerosol mass of more than 60 % over the remote ocean (Brüggemann et al., 2018).

Organic compounds are highly concentrated at the sea-surface microlayer (SML) or as surfactant coatings on cloud droplets (Carpenter and Nightingale, 2015). The air-water interface is ubiquitous in the environment and frequently exposed to the atmosphere and/or solar light, making photochemical interactions highly probable (Liss and Duce, 2005), particularly in the presence of light-absorbing compounds, such as chromophoric dissolved organic matter, which is more concentrated at surfaces than in bulk (Carlson, 1983; Carlson and Mayer, 1980). Organic coatings on water surfaces are a significant source of atmospheric aerosols, either through direct emission to the atmosphere, such as sea spray, or indirect emission through the generation of new products from photo interactions on the surface exposed to solar radiation. The presence of organic coatings on water surfaces can increase the concentration of natural photosensitizers, leading to an increased rate of photochemical reactions (Tinel et al., 2016).

Natural bodies of water, including lakes, rivers, and oceans, exhibit varying pH values and mineral contents, which are influenced by a range of atmospheric, geological, and biological processes. Typically, the pH of natural water bodies varies between 6 and 9 (Dickson, 1993; Jiang et al., 2019) and the salinity can range between 0.5 ppt, for fresh water, and 35 ppt, for ocean (Millero et al., 2008). However, certain factors, such as acid rain or specific geological formations, can cause the pH and salinity to cross these limits. Moreover, the presence of minerals such as calcium, magnesium, sodium, chloride, and sulfate can influence the salinity and also pH (Covington and Whitfield, 1988; Marion et al., 2011), which thus contributes in two ways to the surface activity of the organic compounds. The mineral content and pH of the natural bodies of water play a vital role in their

https://doi.org/10.5194/egusphere-2025-1233
Preprint. Discussion started: 26 March 2025


chemical and physical processes such as rock weathering, mineral precipitation, gas solubility, corrosion, biological shell formation, and water hardness (Morgan, 1995).

Prior reports on the existence and significance of organic layers at air-water interfaces, such as the SML (Bernard et al., 2016; Ciuraru et al., 2015; Mmereki and Donaldson, 2002; Tinel et al., 2016) and sea spray (Sellegri et al., 2006; Wilson et al., 2015), emphasized the need to investigate this critical interface, particularly at the molecular level and under atmospheric conditions. Despite numerous studies aimed at investigating the emission and uptake of gases and aerosols (e.g. VOCs, secondary organic aerosol (SOA) particles, and trace gases) in the atmosphere, limited information is available on the molecular composition and structure of surface entities (e.g. adsorbed on cloud droplets or sea surfaces) and their role in influencing interactions. There is a continued urgency to comprehend fundamental processes at this interface, as it is widely known that atmospheric reactions are highly dependent on the interfacial layers.

The air-water surface interactions occur in a variety of bodies of water and involve both biogenic and abiotic emissions (Bernard et al., 2016; Brüggemann et al., 2018), with organic materials from the SML being emitted into the atmosphere through bubble bursting and forming sea-spray aerosols (Gantt and Meskhidze, 2013; Sellegri et al., 2006). These organic materials can be oxidized in the air and contribute to the creation of SOAs, which can then act as ice nuclei in mixed-phase clouds and high-altitude ice clouds (Liss and Duce, 2005). In recent years, the study of the air-water interface has received increasing attention in atmospheric research (Alpert et al., 2017; Bernard et al., 2016; Carpenter and Nightingale, 2015; Ciuraru et al., 2015; Gantt and Meskhidze, 2013; Liss and Duce, 2005; Sellegri et al., 2006; Tinel et al., 2016; Wilson et al., 2015). Tinel et al. (2016) revealed that the photosensitized chemistry of fatty acids at the air-water interface leads to unique interactions under atmospheric conditions (Tinel et al., 2016). The authors examined the photodegradation of Nonanoic acid (NA), a simple fatty acid, in the presence of two natural photosensitizers, 4-benzoylbenzoic acid (4-BBA) and imidazole-2-carboxaldehyde. The study showed that organic coatings on the water surface can enhance the concentration of natural photosensitizers at the air-water interface, promoting specific photochemical reactions that impact the composition and concentration of VOCs emitted into the atmosphere. Additionally, the authors reported the production of SOA particles following photochemical reactions and ozonolysis of saturated long-chain fatty acids and alcohol surfactants at the water surface (Alpert et al., 2017).

The prior experimental studies have largely utilized chemical, elemental and linear spectroscopic methods (such as UV-visible absorption, laser-induced fluorescence, and mass spectrometry). Molecular-level spectroscopic data on air-water interactions under atmospheric conditions are scarce, with limited in-situ information on molecular alignment, water bonding, and the formation or

https://doi.org/10.5194/egusphere-2025-1233
Preprint. Discussion started: 26 March 2025


degradation of chemical functional groups at the air-water interface. A molecular-level understanding of gas-liquid interactions under atmospheric conditions and the factors that influence the reaction mechanisms is critical to predicting the formation and degradation of aerosols, and is therefore of fundamental importance.

In this work, we combine sum-frequency generation (SFG) spectroscopy and mass spectrometry (MS) to probe the interfacial and bulk-phase photoproducts, respectively, of a fatty acid being irradiated with different solar spectra at different pH and salinity at the air-water interface. We studied the photochemical interactions of nonanoic acid (NA) at the water surface in the presence of 4-benzoylbenzoic acid (4-BBA). This system was particularly chosen due to the availability of a reference work where only linear techniques were used to probe the photoproducts in the bulk phases (Tinel et al., 2016). The reference work verified that the interaction takes place at the water surface. Since SFG technique is suitable to probe the surface layer, we applied it here to probe the chemical and structural changes in the system. We detected an aromatic signal by the SFG upon the photoreaction which was not reported by the linear techniques used in the reference work. The changes in the SFG spectra with irradiation depend on the pH of the solution. For the irradiation of the samples we use an LED solar simulator that produces a light spectrum that is closer to the solar spectrum than that of commercially available Xenon lamp that has been used in the reference work. We also studied the effect of pH, starting from a pH similar to the ocean to the normal pH. We found that the solar spectrum, pH and salinity affect the photoreaction rate by interfering mechanisms.

## 2. Experimental procedures

### 2.1 Materials

4-benzoylbenzoic acid (4-BBA, 95 %,) and nonanoic acid (NA, 97 %) were purchased from Sigma Aldrich and Alfa Aesar, respectively. All solutions were prepared using ultrapure water (18.2 MΩ cm; total oxidizable carbon <5 ppb) that was obtained from a Milli-Q Reference A+ (Merck) purification system). Unless mentioned differently, all mixtures examined here are aqueous solutions of 2 mM NA and 0.2 mM 4-BBA and a volume of four milliliters. The solution of 4-BBA was prepared using ultrasonication for three hours and then steering over night at pH 7. The solution of NA was prepared using ultrasonication for one hour. The pH was adjusted using 0.1 M NaOH from Fischer Chemical and controlled with SevenExcellence pH/Cond meter S470 from METTLER TOLEDO. Lab experiments were conducted under either synthetic air (ALPHAGAS$^{TM}$, 20.5 ± 0.5 % $O_2$ in $N_2$) or Nitrogen gas (99.9999 %) from Air Liquid. The exact conditions for each experiment can be found in the SI.

https://doi.org/10.5194/egusphere-2025-1233
Preprint. Discussion started: 26 March 2025


## 2.2 Photochemical reactor

To study photochemistry under atmospheric conditions, an irradiation source that closely mimics solar light is essential. It should be tunable to simulate different latitudes, altitudes, and seasonal variations, requiring a wavelength range starting at ~275 nm, adjustable intensity, and homogeneous illumination. For this purpose, a compact custom-built LED-based solar simulator, the "Atmospheric Surface-Science Solar Simulator", was developed. The device is optimized to irradiate a 30 mm diameter sample area from a 50 mm distance, ensuring controlled photochemical reactions. The spectral characteristics of the simulator, including its spectral overlap with solar radiation and intensity adjustments, were determined using a calibrated spectrophotometer and a custom-built variable current source. Additional technical details, including LED spatial distribution, spectral comparisons, and homogeneity calibration, are provided in the Supporting Information (SI).

## 2.3 SFG spectroscopy

Surface sum-frequency generation (SFG) spectroscopy is based on second-order nonlinear optical effect that in dipole approximation only occurs where the inversion symmetry is broken which is always the case at interfaces between two phases (Miranda and Shen, 1999; Zhang et al., 1994). SFG is generated by a temporal and spatial overlap of two different frequency light pulses (usually visible and a tunable IR) at an interface between two isotropic media. It provides information about the interface by probing the individual species from their IR vibrational absorption (Shen, 1989). SFG has proven effective in probing aqueous solutions containing soluble ionic and molecular species, and in determining the role of these substances in changing the water structure at the interface (Schultz et al., 2002; Shultz et al., 2000). Surfactants partition to the interface and can displace or bind water into hydrated complexes. Various SFG investigations on air-water interfaces have centred on examining organic surfactants adsorbed at the water surface (Backus et al., 2012; Doughty et al., 2016; Ghosh et al., 2009; Henry et al., 2003; Rao et al., 2011; Truong et al., 2019; Varga et al., 2005). However, it is mandatory to focus on studies that include atmospherically relevant substances under atmospheric conditions.

The description of the SFG spectrometer used in this study can be found elsewhere (García Rey et al., 2019). The irradiation and ray geometry used in the present work are shown in SI. Details of the SFG experiments and data analysis can be found in the Supporting Information (Sect. S3). Table S2 lists the experimental conditions of all SFG experiments conducted in this work. At first glance, due to the distinguished feature of SFG as a sub-monolayer surface-sensitive technique, we realized that the delivered 4-BBA contained surface-active contaminants. The purple spectrum in Fig. S6 shows vibrational bands in the CH region detected at the surface of a 0.2 mM aqueous solution of 4-BBA.

https://doi.org/10.5194/egusphere-2025-1233
Preprint. Discussion started: 26 March 2025


These bands are attributed to surface active organic contaminants in the solution. 4-BBA is not surface active (Mora Garcia et al., 2021) and there are no free CH bonds that could produce the CH-vibrations. To purify the 4-BBA, it was recrystallized twice from Ethanol. The green curve in Fig. S6 shows the SFG spectrum of 4-BBA aquatic solution after the recrystallization. It is worth mentioning that we tested samples from different providers, including the provider mentioned in the reference work (Tinel et al., 2016), and found that 4-BBA was never delivered pure enough to not show surface-active contaminants. The contamination in the 4-BBA should be considered when comparing our results with those in the reference work.

### 2.4 Mass spectrometry

The analysis of liquid-phase products was carried out using the Filter Inlet for Gas and Aerosols (FIGAERO, Aerodyne Inc.) in combination with a high-resolution time-of-flight chemical ionization mass spectrometer (HR-ToF-CIMS, Aerodyne Inc.), employing $I^-$ as the ionization reagent. A 2.5 µL liquid sample was applied to a PTFE filter via a syringe and subsequently subjected to thermal desorption in FIGAERO-CIMS. Ultra-high-purity nitrogen served as the carrier gas, facilitating desorption as the temperature was gradually increased from 296 K to a peak of 473 K over 35 minutes. The total liquid-phase signal for each compound was determined by integrating its thermal desorption profile (thermogram). Data processing was performed using Tofware software v3.1.2, with mass-to-charge ratios adjusted by subtracting the reagent ion I−. To enable comparisons, all ion signals were normalized to $10^6$ cps $I^-$. Proton-transfer-reaction time-of-flight mass spectrometer (PTR-ToF-MS 4000, Ionicon Analytic GmbH) was utilized to measure the concentrations of gas-phase compounds. The data was analyzed by PTR viewer 3.3.12. The gas phase was sampled by a syringe and transferred to the PTR-MS. Table S3 lists the experimental conditions of all MS experiments conducted in this work. Since the photoreactor cannot be considered completely air-tight the measured concentrations cannot be converted into absolute yields of the gas phase reaction products. Results of the mass spectrometry given in the results section were subtracted by the background signals measured in the reference experiment MS_BG1.

## 3 Results

### 3.1 SFG at the air-liquid interface

Figure 1 shows the SFG spectra at vapor-water interface for NA, (a), and 4-BBA, (b), in dark conditions and after exposure to AM0 light (solar radiation spectrum before absorption by the atmosphere). AM0 was chosen because it includes the maximum portion of sun UV that can lead to

https://doi.org/10.5194/egusphere-2025-1233
Preprint. Discussion started: 26 March 2025


photo-induced chemistry in the atmosphere. Solution's pH was adjusted to pH 8, which is the approximate pH value of the ocean (Jiang et al., 2019). As the SFG spectra in Fig. 1 show, no considerable changes were observed upon exposure to AM0 light, particularly for NA. The changes in SFG spectra of air-water interfaces using 4-BBA solutions were within the signal-to-noise upon different exposure to AM0 irradiation. Although this is indicative for a neglectable influence of AM0 irradiation on pure 4-BBA solutions, a small drop in the SFG signals from the air-water interface after 30 min of irradiation time and a subsequent increase in the signal can be seen.

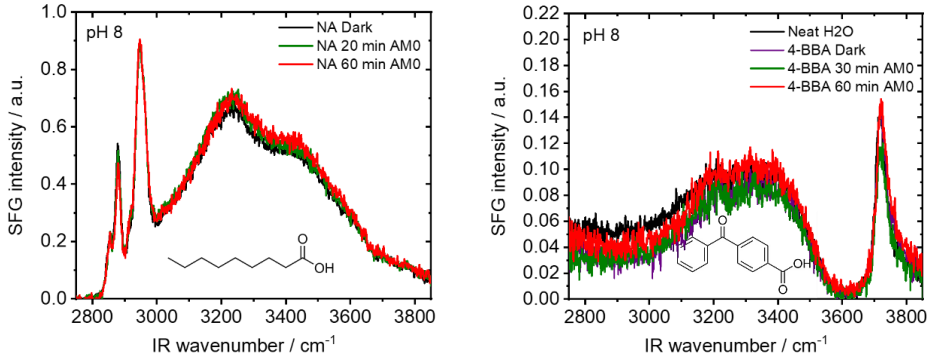


**Figure 1: SFG at (a) air-water interface for NA (2mM), and (b) 4-BBA (0.2mM) as a function of time in dark conditions and after exposure to AM0 light. Both solutions were adjusted to pH 8.**

Figure 2a shows the SFG spectra from air-water interfaces for mixtures of NA and 4-BBA at a solution pH 8 as a function of time after which the interface was established, while the samples were continuously kept in the dark conditions (no light exposure). There is a visible change in the signal along the whole frequency range. At the beginning of the experiment, the SFG spectrum of the mixture shows a vibrational band that is attributable to the so-called dangling OH (~3700 $cm^{-1}$) mode from water molecules at the interface that have one non-hydrogen bonded OH group pointing into the vapor phase (Sovago et al., 2008). Additional broad OH bands from interfacial water are centered at ~3450 $cm^{-1}$ and ~3240 $cm^{-1}$, while CH vibrational bands ($CH_3$ Fermi peak at 2946 $cm^{-1}$, $CH_2$ Fermi peak at 2917 $cm^{-1}$, $CH_3$ symmetric-stretch 2885 $cm^{-1}$, and $CH_2$ symmetric-stretch at 2858 $cm^{-1}$) (Lu et al., 2005; MacPhail et al., 1984; Snyder et al., 1982). The $CH_2$ Fermi resonance appears as a shoulder next to the $CH_3$ Fermi peak and could be located by the SFG data fitting as shown in the SI. Close inspection of Fig. 2a reveals that the dangling OH band decreased with time to neglectable intensity after ~50 min under dark conditions. We have fitted the dangling OH band for different times and present the results in Fig. S8 (Supporting Information) clearly showing the decay of dangling OH intensity as a function of time. These changes reflect the adsorption rate and structuring

https://doi.org/10.5194/egusphere-2025-1233
Preprint. Discussion started: 26 March 2025


of NA at the air-water at pH 8, which are accompanied by a slight increase of the OH bands at 3450 $cm^{-1}$ and 3240 $cm^{-1}$ from interfacial water (Fig. 2a and Fig. S9), indicating a relatively slow restructuring of water molecules at the interface. At the same time, the $CH_3$-SS peak intensity, which we assume to be proportional to the number of interfacial NA, slightly increases with time when the sample was kept in the dark (see Fig. S10). The trivial changes in the CH bands are expected due to ongoing interface adsorption until equilibrium is reached and is not expected to be caused by photochemistry as all the experiments so far were performed under dark conditions.

Figure 2b shows SFG spectra at air-water interface for the mixture which were first equilibrated for 80 min in dark and, then, exposed for different times to AM0 irradiation. There are two observed phenomena: 1) The appearance of a new narrow band at ~3070 $cm^{-1}$ which can be ascribed to a =C–H stretch in an aromatic compound (Gautam et al., 2000; Hardt et al., 2024) A bidirectional change in the peak intensity of all bands. This means that two opposing processes occur simultaneously at the interface, as illustrated in the Discussion section. The appearance of the new band is expected and can be attributed to the photochemistry taking place at the water surface. However, the behavior of the water bands is questioned.

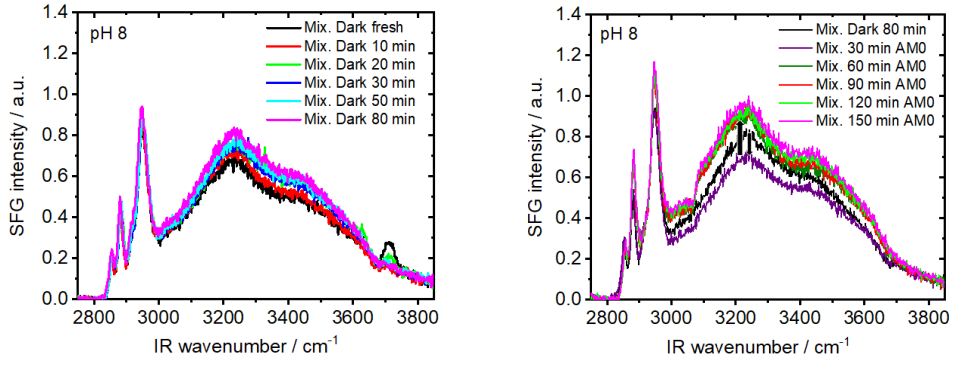


**Figure 2: Changes of SFG spectra at air-water interface of a 2 mM NA mixture with 0.2 mM 4-BBA at pH 8 as a function of time under (a) dark conditions as well as for (b) irradiation with AM0.**

One possible reason for the anomalous amplitude changes of the water bands under light conditions, as well as the slight change under dark conditions, is the change of pH of the bulk solution. Indeed, we found that the pH decreases with time for the same mixture under dark and light (UV) conditions until the pH stabilizes around a neutral pH, Fig. S12 Under dark conditions, the solution's pH decreases exponentially with time, however, under irradiation conditions, the pH also decreases but with a higher rate. The decrease in pH under dark conditions is simply due to the carbonation of the solution under room conditions as was observed for a pH 8 solution without the mixture, orange curve

https://doi.org/10.5194/egusphere-2025-1233
Preprint. Discussion started: 26 March 2025


Fig. S12. The enhanced decrease in pH upon UV irradiation is only observed at pH 8 of the mixture solution which indicates a contribution from the reaction products. On one side, the water molecules at the surface are directly affected by the surface charge (Nihonyanagi et al., 2013). On the other side, the change in bulk pH changes the concentration of the NA at the surface which in turn indirectly affects the water structuring. The influence of pH on the detected SFG signal will be discussed in the Discussion section.

To eliminate the complexity of pH effect and to reduce the number of variables, we examined the same system but at a moderate pH value (5.4 to 5.6) which is not very sensitive to carbonation and other factors that may change the pH value over time (green curve Fig. S12). Indeed, the behavior of water bands (increase under dark conditions and decrease and then increase under light conditions) was not observed for low pH solution, Fig. 3. In addition, the dangling OH, which characterizes the neat air-water interface, was not observed at low pH in the first dark measurement. This means that the spread of NA on the surface was faster than that in the case of high pH. This is in line with the dependency of the dissociation constant on pH. At intermediate pH, a considerable portion of negatively charged molecules are neutralized to create neutral fatty acid molecules, which have a much greater adsorption constant than their anionic counterparts (Badban et al., 2017). The aromatic CH stretching band at ~3070 $cm^{-1}$ was visible after 60 min which is about the same time when it appeared for solution with pH 8 (Fig. 2b).

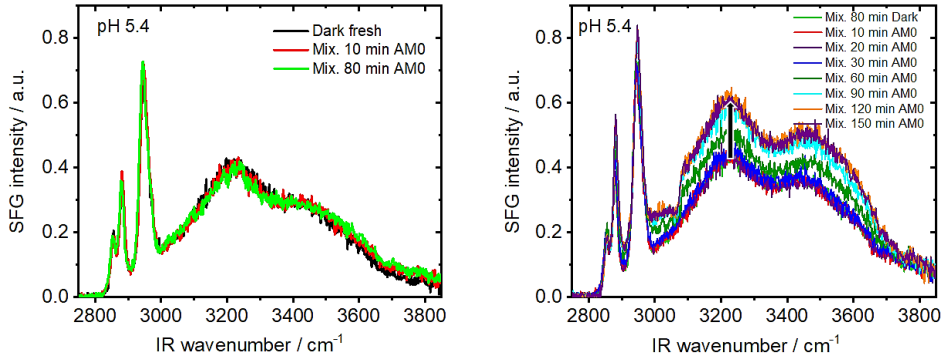


**Figure: 3.SFG spectra at air-water interface of the mixture, (2 mM NA + 0.2 mM 4-BBA) at pH5.4, under dark (a) and irradiation with AM0 (b) conditions.**

To quantify the influence of the solar radiation spectrum on the photo reaction, we probed the effect of three irradiation conditions; AM0, AM1 (spectrum of solar light after traveling through the atmosphere), and solely the UV portion of AM0 for 90 min on the same mixture. The results in Fig. 4a show that the solution exposed to AM0 exhibited a strong aromatic band and a noticeable increase

https://doi.org/10.5194/egusphere-2025-1233
Preprint. Discussion started: 26 March 2025


in water bands within one and a half hours. In contrast, the solution exposed to AM1 shows very little presence of an aromatic band and a slight increase in water bands after the same irradiation time, Fig. 4b. Irradiating the solutions with only the UV part of AM0 shows a clear aromatic band with almost no change in the water bands, Fig. 4c.

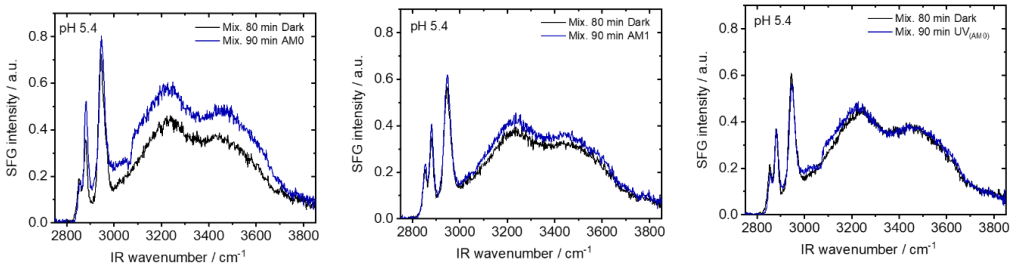


(a) AM0 (b) AM1 (c) UV of AM0

**Figure 4: SFG spectra at air-water interface of 2 mM NA aqueous mixtures with 0.2 mM 4-BBA at a pH of 5.4, before and after irradiation with (a) AM0, (b) AM1 and (c) UV part of AM0.**

Finally, solutions at pH 5.6 were irradiated by ten different wavelengths for the same time (18 h) and an SFG spectrum was collected for the fresh solution, then after 0.5, 3 and 18 h of irradiation time. The intensity of each wavelength was adjusted to be equivalent to that of the corresponding wavelength in the AM0 spectrum. The SFG spectra are shown in Fig. 5 and Fig. S11. Both figures correspond to the same set of measurements, but with different display formats to illustrate the change in the aromatic band and the changes in water bands respectively. Figure 5 shows that the aromatic band was visible only in the short UV wavelengths, mainly 280, 310, and 345 nm. For the sample irradiated by 280 nm, the aromatic band was visible already after three hours although it has the lowest intensity in the solar spectrum. Figure S11 shows that the water bands were changing differently with different wavelengths. The spectrum after 0.5 h has been omitted from Fig. S11 for clarity reasons. In most of cases, the change in the aromatic CH stretching band was stronger at shorter wavelengths. The general trend of the band amplitudes looks almost similar but with faster changes at shorter wavelengths. However, in some cases it is different. For example, the solution irradiated with 365 nm shows a change in the water band after three hours similar to that of the solution irradiated with 280 nm. Except for the 280 nm, there is always a decrease (at three hours) and then an increase (at 18 h) in the water bands with irradiation. Most likely the solution irradiated with 280 nm went through the same reaction path as for the other wavelengths but at an earlier time because of a faster photoreaction rate. The individual irradiation wavelengths have both different wavelengths and intensities which was done on purpose to mimic the corresponding solar irradiance for each wavelength. The SFG study also showed that the salt concentration of the bulk accelerates the photo

https://doi.org/10.5194/egusphere-2025-1233
Preprint. Discussion started: 26 March 2025


reaction (see Sect. S5 and Fig. S14). It is not the focus of this paper to discuss the details of the salinity effect on the photochemistry at this surface, we only register the observed phenomenon.

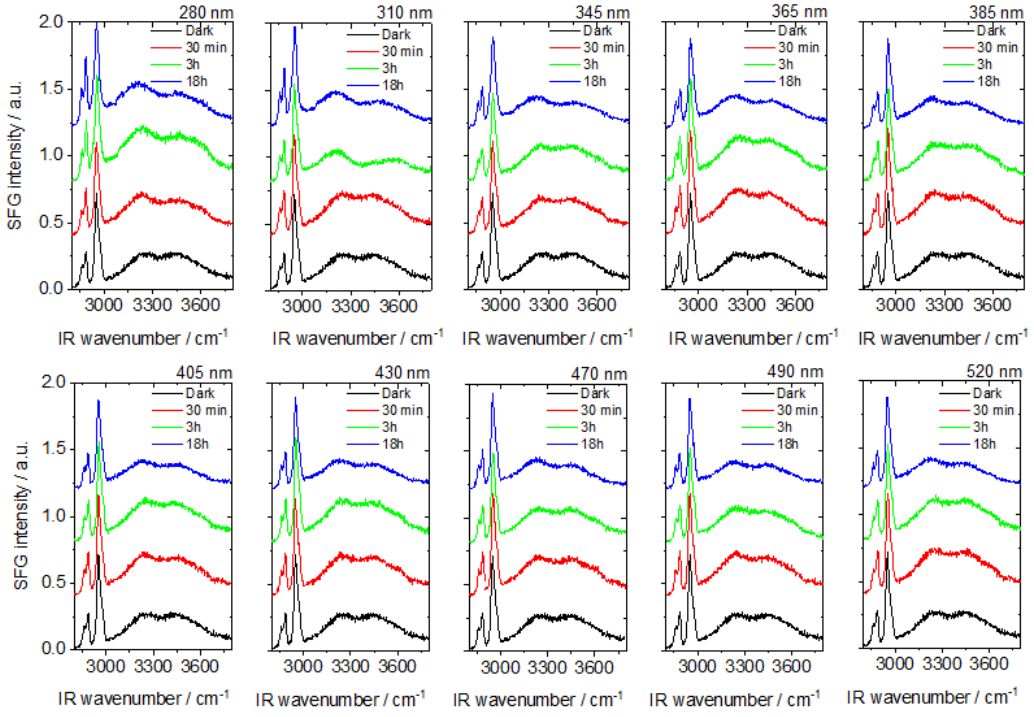


**Figure 5: SFG spectra at air-water interfaces of (2 mM NA + 0.2 mM 4-BBA) mixtures at pH 5.6 after different times of irradiation with different wavelengths. Note that the spectra have a constant with offset.**

## 3.2 Chemical composition of gas and liquid phase

The aromatic compound detected at the air-water interface by SFG spectroscopy is a result of a photoreaction occurring for the studied samples when they are irradiated with UV containing radiation e.g. AM0. As previously mentioned, this surface-active compound and the minute details on pH effect and water band changes were not reported by the linear techniques used in the reference work by Tinel et al., 2016. The reactions in the visible wavelength range were neither expected nor previously reported. Considering these facts and recalling that the mass spectroscopic results in Tinel et al., 2016, although very thorough, were collected from samples irradiated with a commercial Xenon lamp as a light source, and that the 4-BBA sample was not purified as ours, we decided to repeat the mass spectrometry measurements using our solar simulator and purified 4-BBA samples (see experimental details).

https://doi.org/10.5194/egusphere-2025-1233
Preprint. Discussion started: 26 March 2025


### 3.2.1 Aqueous phase analysis

The products of the photochemical reactions of NA were detected under different irradiation and at a fixed pH of ~5.8. Figure 6 shows the evolution of seven main liquid-phase products detected in experiment MS.1 under irradiation with AM0 and in the presence of 4-BBA as photosensitizer: $C_8H_{12}O_4$, $C_8H_{12}O_5$, $C_9H_{10}O_5$, $C_9H_{14}O_3$, $C_9H_{16}O_3$, $C_9H_{16}O_4$, and $C_{10}H_{14}O_4$. The suggested assignments of the detected compounds in the liquid phase are listed in Table S4 of the Supporting Information. Some of the products showed faster production rates during the first hour, while the others showed a slower rate. We do not observe any correlation between the production rate and chain length nor the molecular weight. However, the differences are close to the experimental uncertainties. The sum of all $C_xH_yO_z$ signal intensities in the liquid phase shows a linear relation with the time of irradiation, Fig. 6. Figure 7 shows the ratio of signals detected for the main liquid-phase photoproducts of the mixture (NA + 4-BBA) versus the signals detected in the absence of 4-BBA with irradiation of AM0 and in the presence of synthetic air. The results show the largest promotion in the formation of $C_8H_{12}O_4$, $C_9H_{10}O_5$ and $C_9H_{16}O_3$ in the presence of 4-BBA.

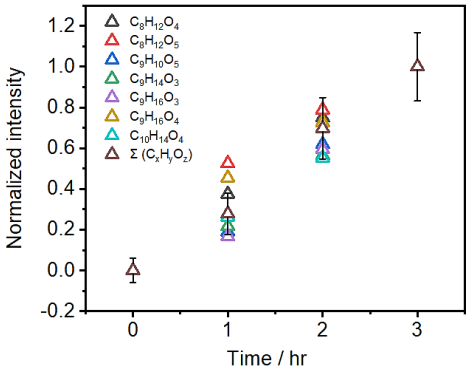


**Figure 6: Concentrations of each photoproduct as a function of exposure times to AM0 (Exp. MS.1) normalized to sum the of all products Σ($C_xH_yO_z$) signal intensities in the liquid phase.**

To examine the role of oxygen in the reactions, we repeated the AM0 experiment with pure nitrogen, instead of the synthetic air, and deoxygenated liquid solutions (Exp. MS.3). The solution was deoxygenated by bubbling with nitrogen for 10 min and the measuring cell was purged before closing it hermetically. Figure 8 shows the ratio of signals detected in the presence of synthetic air versus those in the presence of $N_2$. The results show that the presence of oxygen causes an increase of $C_8H_{12}O_5$, $C_9H_{14}O_3$, $C_9H_{16}O_3$, and $C_9H_{16}O_4$ by a factor of 10 to 12. The presence of oxygen shows only a limited promotion on the formation of $C_8H_{12}O_4$ (factor of ~2), but a significant promotion on the formation of $C_{10}H_{14}O_4$ (factor of ~19) and $C_9H_{10}O_5$ (factor of ~34). This emphasizes the vital role of dissolved oxygen in the natural bodies of water to develop multiple pathways of interactions.

https://doi.org/10.5194/egusphere-2025-1233
Preprint. Discussion started: 26 March 2025


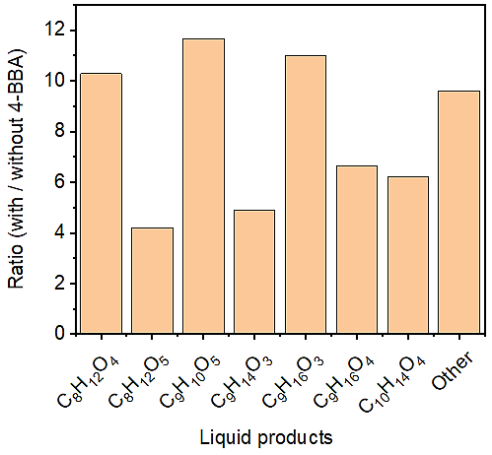


**Figure 7: Ratio of the signal detected in the presence of 4-BBA to the signal observed without 4-BBA for the main detected photoproducts in the aqueous phase for an aqueous solution with NA with irradiation of AM0 under synthetic air environment.**

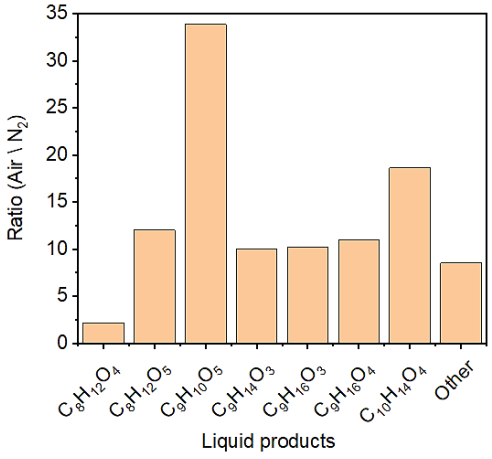


**Figure 8: Ratio of the signal detected in the presence of 4-BBA and synthetic air compared to those in the absence of oxygen in gas and liquid phase for the main photoproducts detected in the aqueous phase, after irradiation with AM0 for three hours.**

Finally, we compare the product formation under AM0 and AM1 to that under sunlight. Figure 9 shows the ratios of the photo products for the mixture irradiated with AM0 (Exp. MS.1) and with real sun light during a clear sunny day in Karlsruhe, Germany, 1st June 2023 from 11 am to 2 pm (Exp. MS.8) versus irradiation with AM1 (Exp. MS.2). The day and time were chosen to guarantee minimal changes in the solar radiation spectrum. With stronger UV light at AM0, the formation of major aqueous photoproducts was promoted, with the increase of total $C_xH_yO_z$ signal by a factor of about 2.4 compared to that at AM1. The same main set of photoproducts observed under artificial irradiation in the laboratory were also detected under sunlight. After being irradiated by real solar light for three

https://doi.org/10.5194/egusphere-2025-1233
Preprint. Discussion started: 26 March 2025


hours, the total $C_xH_yO_z$ signal observed was ~0.9 of that observed at AM1. Hence, our experiments with AM1 irradiation are indeed comparable to typical atmospheric conditions at earth surface. The relative product fractions for irradiation with sunlight are very similar to those of the lab irradiation and mostly lie between those of irradiation by AM0 and AM1. The fractions of the photoproducts that constitute of 2 % or more of the total products (i.e. $C_9H_{16}O_4$, $C_{10}H_{14}O_4$, $C_8H_{12}O_4$, $C_9H_{16}O_3$, and $C_9H_{10}O_5$, ascendingly) are closer to those of AM1 which is consistent and emphasis the capability of our homemade light source to simulate ambient solar radiation.

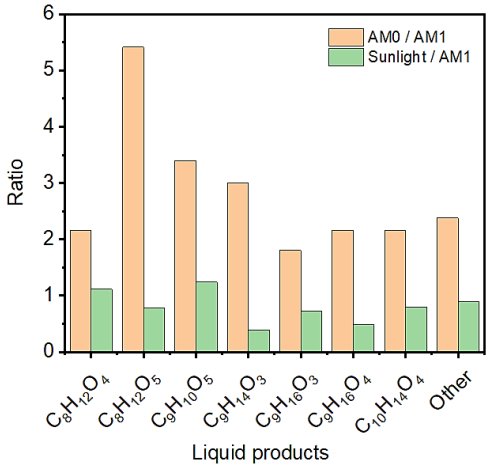


**Figure 9: Ratio of the compounds detected with AM0 or sunlight versus the signal with AM1, for a NA aqueous solution with 4-BBA after irradiation for three hours.**

The SFG spectra of solutions irradiated with different single wavelengths, Fig. 5, exhibited varying changes in the water bands regardless of the appearance of the aromatic CH stretching band. To precisely quantify the effect of different irradiation wavelengths on the generation of photoproducts, we examined the solution mixture irradiated with four selected single wavelengths in the UV and Visible part of the spectrum. Figure 10 shows the total $C_xH_yO_z$ signal detected in the liquid phase for different irradiation conditions as illustrated under the x-axis.

To address the wavelength dependence of the photoproducts further, we plot the fraction of the three most dominating products, namely $C_8H_{12}O_4$, $C_9H_{10}O_5$, and $C_9H_{16}O_3$, versus irradiation wavelength in Fig. 11. The fractions of $C_8H_{12}O_4$ and $C_9H_{16}O_3$ increase with longer wavelength while the fraction of the $C_9H_{10}O_5$ increases with shorter wavelength indicating two different mechanisms as will be described in the discussion section.

https://doi.org/10.5194/egusphere-2025-1233
Preprint. Discussion started: 26 March 2025


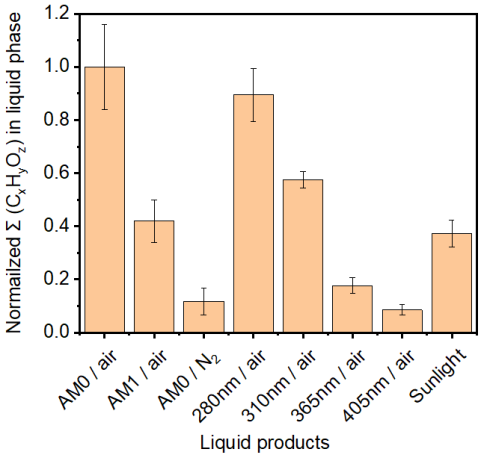


**Figure 10: Normalized total $C_xH_yO_z$ signal in aqueous phase at different irradiation conditions. [Exps. MS.1 to MS.9 (SI)]**

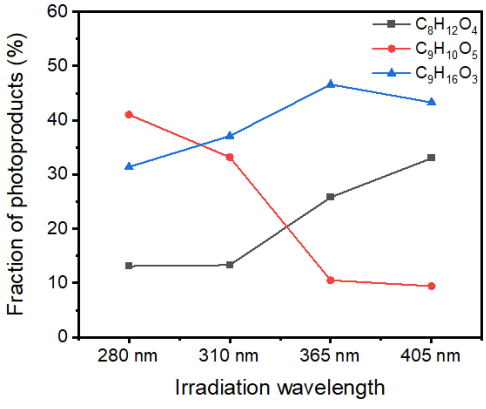


**Figure 11: The fraction of photoproducts versus wavelength for the three most dominating products, ($C_8H_{12}O_4$, $C_9H_{10}O_5$, and $C_9H_{16}O_3$) after irradiation with 280, 310, 365, and 405 nm for three hours.**

### 3.2.2 Gas phase analysis

Examining the gas phase is important to detect the volatile photoproducts. A series of compounds, such as $C_4H_8$ (butene), $C_4H_8O$ (butanal), $C_5H_{10}$ (pentene), $C_5H_{10}O$ (pentanal), $C_6H_6$ (benzene), $C_7H_8$ (toluene), $C_7H_6O$ (benzaldehyde), $C_8H_{16}O$ (octanal), as well as some undefined fragments such as $C_6H_5$ and $C_7H_6$ were detected in the gas phase (see Table S5). Only two of which showed a significant increase compared to the background experiments (BG1-3). Figure 12 shows the normalized signals of the two main gas-phase compounds: benzene ($C_6H_6$) and benzaldehyde ($C_7H_6O$) under different irradiation conditions. When NA was irradiated in the absence of 4-BBA, the signal from both products remained at background levels. However, when either the mixture or 4-BBA alone was irradiated with AM0, both compounds exhibited strong signals. This clearly indicates that, in addition

https://doi.org/10.5194/egusphere-2025-1233
Preprint. Discussion started: 26 March 2025


to the previously reported photochemical reaction of NA in the presence of 4-BBA, 4-BBA itself undergoes photolysis under UV irradiation. For other gas-phase compounds detected in this study, no significant differences were observed between the normal irradiation experiments and the background experiments.

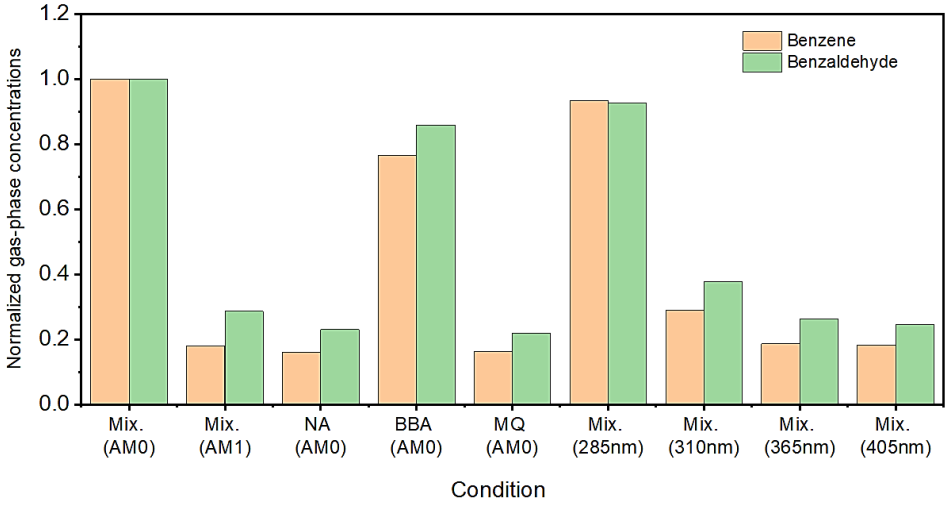


**Figure 12: MS signals of benzene and benzaldehyde detected in the gas phase for different solutions under different irradiation conditions for three hours. Signals are normalized to that of the mixture under AM0 irradiation condition.**

## 4. Discussion

As previously mentioned the aim of this work was to explore on the molecular level the photochemistry of the organic surfactant NA at the air-water interface in the presence of the photosensitizer 4-BBA. For that, we have used environmental conditions that are similar to the real environment at sea water and droplets in the atmosphere. We examined three irradiation conditions which are equivalent to solar irradiation at the top of atmosphere and near the sea level. We have also examined pH values which are representative of most natural water bodies (~pH 6 to 8). In our study we utilized an LED solar simulator that produces a light spectrum that is closer to the solar spectrum than that of the Xenon lamp used in the reference work (Tinel et al.).

### 4.1 Influence of the irradiation spectrum

The real solar radiation spectrum depends on weather, latitude, altitude and season. These factors qualitatively and quantitatively affect the photochemistry in the hydrosphere. The irradiation of the mixture with AM0 which includes wavelengths lower than 310 nm yielded the largest quantity of surface and bulk phase photoproducts among all the experiments. SFG spectra presented above

https://doi.org/10.5194/egusphere-2025-1233
Preprint. Discussion started: 26 March 2025


indicate strong signals at 3070 $cm^{-1}$ which are indicative for aromatic moieties at the air-water interface formed after continuous irradiation with AM0 for 90 min (Fig. 4a). Changes in the CH bands also point to variations of the chemical composition in the topmost layer at the air-water interface. In addition, also OH stretching modes from interfacial water increased significantly after irradiation with AM0. We propose that the latter is associated to the formation of hydrocarbons that can change the structure of hydrogen-bonded water molecules at the interface upon their formation which is triggered by irradiation of the samples with e.g. AM0. Irradiation with AM1, Fig. 4b, showed a weaker effect compared to that after the irradiation with AM0 which is in line with the reduced intensities of all spectral wavelengths, particularly the UV part. However, experiments where the wavelength and/or the spectrum of the light irradiation was systematically varied provided evidence that only the UV contribution to AM0, Fig. 4c, is responsible for the observed photochemical reaction of NA mixtures with 4-BBA. Particularly, aromatic products are produced in the presence of UV light by the photolysis of 4-BBA, as will be discussed in detail in the next section. This means that the main effect producing the aromatic compound comes from the UV part of the solar spectrum and such a photoproduct would be produced in the atmosphere (e.g. in cloud droplets) rather than at the sea surface. On the other hand, the visible part of the spectrum produces fewer photoproducts.

Testing the effect of individual wavelengths for longer times of irradiation (up to 18 h), Fig. 5 confirmed the responsibility of the UV light for the generation of the aromatic compound(s). It also showed that the effect of different wavelengths has different weights due to the changes in intensity and wavelength. The shorter wavelength and/or higher intensity have a stronger effect on both the surface-active and bulk species. The results highlight the significant impact of solar spectrum composition on reaction pathways. They also emphasize the importance of incorporating these variations into the photochemical models used in atmospheric science for more accurate predictions of the complex chemical interactions that occur in the atmosphere (Photochemical Air Quality Modeling; Xing et al., 2022).

## 4.2 Evolution of pH values

For solutions with a higher pH value of 8, a faster decrease in pH in the presence of 4-BBA after switching the UV light on (blue curve in Fig. S12). Under UV light irradiation, the 4-BBA molecule absorbs energy, leading to excitation. The excited state can undergo decarboxylation, where the carboxyl group (-COOH) is lost as carbon dioxide ($CO_2$), resulting in the formation of benzene and a carboxylic acid radical. The carbonation is the dissolution of carbon dioxide ($CO_2$) in water to form carbonic acid ($H_2CO_3$), which can further dissociate into bicarbonate ($HCO_3^-$) and carbonate ($CO_3^{2-}$) ions. The carbonation process is primarily influenced by the concentration of dissolved $CO_2$ in water

https://doi.org/10.5194/egusphere-2025-1233
Preprint. Discussion started: 26 March 2025


and the partial pressure of $CO_2$ in the surrounding atmosphere. The pH of the solution can indirectly affect carbonation by influencing the equilibrium between carbonic acid and its dissociation products. The fast decrease in pH value under UV light for a solution with an initial ~pH 8 and containing 4-BBA is a laboratory issue due to the relatively high 4-BBA concentration in a limited sample volume. In nature, this effect is negligible, e.g. in large water reservoirs, but could become relevant, e.g. for cloud droplets.

To understand the indirect effect of pH change on the SFG signal, we have to recall that the balance between the hydrophobic tail and the hydrophilic head controls the adsorption of surfactants. While hydrophobicity is directly connected with hydrocarbon length, hydrophilicity is mostly unquantified (Rosen and Kunjappu, 2012). The hydrophilicity of head groups is qualitatively related to the solvation and solubility. Thus, a nonionized state would be less hydrophilic than an ionized state because it would be less soluble. Normally, NA is only partially dissociated. The change in pH at a constant concentration of NA changes the concentration of NA at the surface and hence the surface pressure (Luo et al., 2020). Although the relationship between the surface pressure and the SFG signal at the air-water interface is not well established, it is confirmed that the SFG signal may increase or decrease with surface pressure depending on a number of factors, such as the composition and arrangement of the molecules at the interface, the polarization of the incident light, and the concentration of adsorbed species (Feng et al., 2016). A side effect of pH change during the experiment is the change in the degree of protonation and deprotonation of 4-BBA at different pH values which affects its absorbance spectra (see Fig. S13) (Karimova et al., 2023). This increases the complexity of the photoreaction if the pH value is not constant during the irradiation process.

## 4.3 Reaction mechanism for the formation of major products

In all MS experiments, $C_8H_{12}O_4$, $C_9H_{10}O_5$, and $C_9H_{16}O_3$ were the most abundant products detected in the liquid phase. However, the fractions of the liquid-phase compounds varied under different irradiation conditions, Fig. 13a to h. For $C_9H_{16}O_3$, which was formed through $RO_2$ radical reactions after hydrogen abstraction on NA (Tinel et al., 2016), the fraction in total liquid-phase $C_xH_yO_z$ was higher with irradiation of AM1 than AM0 Fig. 13a and b. This stands in agreement with the measurement with irradiation from 280 nm to 405 nm, Fig. 13e to h. With more UV at 280 nm and 310 nm, $C_9H_{16}O_3$ accounted for about ~31 % and ~37 % of total $C_xH_yO_z$, respectively; while with less UV at 365 nm and 405 nm, the fractions of $C_9H_{16}O_3$ increased to ~47 % and ~43 %, respectively. In contrast, the fraction of $C_9H_{10}O_5$ in total liquid-phase $C_xH_yO_z$ decreased from ~41 % at 280 nm to ~9 % at 405 nm. We also observed a higher fraction of ~34 % for $C_9H_{10}O_5$ at AM0, and a lower fraction of ~24 % at AM1. For $C_9H_{16}O_3$, the signals in the reference experiments in the absence of

https://doi.org/10.5194/egusphere-2025-1233
Preprint. Discussion started: 26 March 2025


NA or 4-BBA were similar to that in the reference experiment in the absence of both NA and 4-BBA. However, we observed significant formation of $C_9H_{10}O_5$ in the experiment of 4-BBA alone, in which the intensity of $C_9H_{10}O_5$ was about half of that in the mixture of NA and 4-BBA experiment, suggesting that $C_9H_{10}O_5$ is very likely to be an aromatic compound formed through 4-BBA irradiation and the presence of NA could promote its formation. This conclusion is consistent with the presence of two different reaction mechanisms as inferred from Fig. 11. $C_8H_{12}O_4$ is a major product from the photoreaction of NA, and there is less dependence of the formation of $C_8H_{12}O_4$ on oxygen compared to other products. This leads to an increase of the fraction of $C_8H_{12}O_4$ in total liquid-phase $C_xH_yO_z$ in $N_2$ experiment, Fig. 13c.

https://doi.org/10.5194/egusphere-2025-1233
Preprint. Discussion started: 26 March 2025


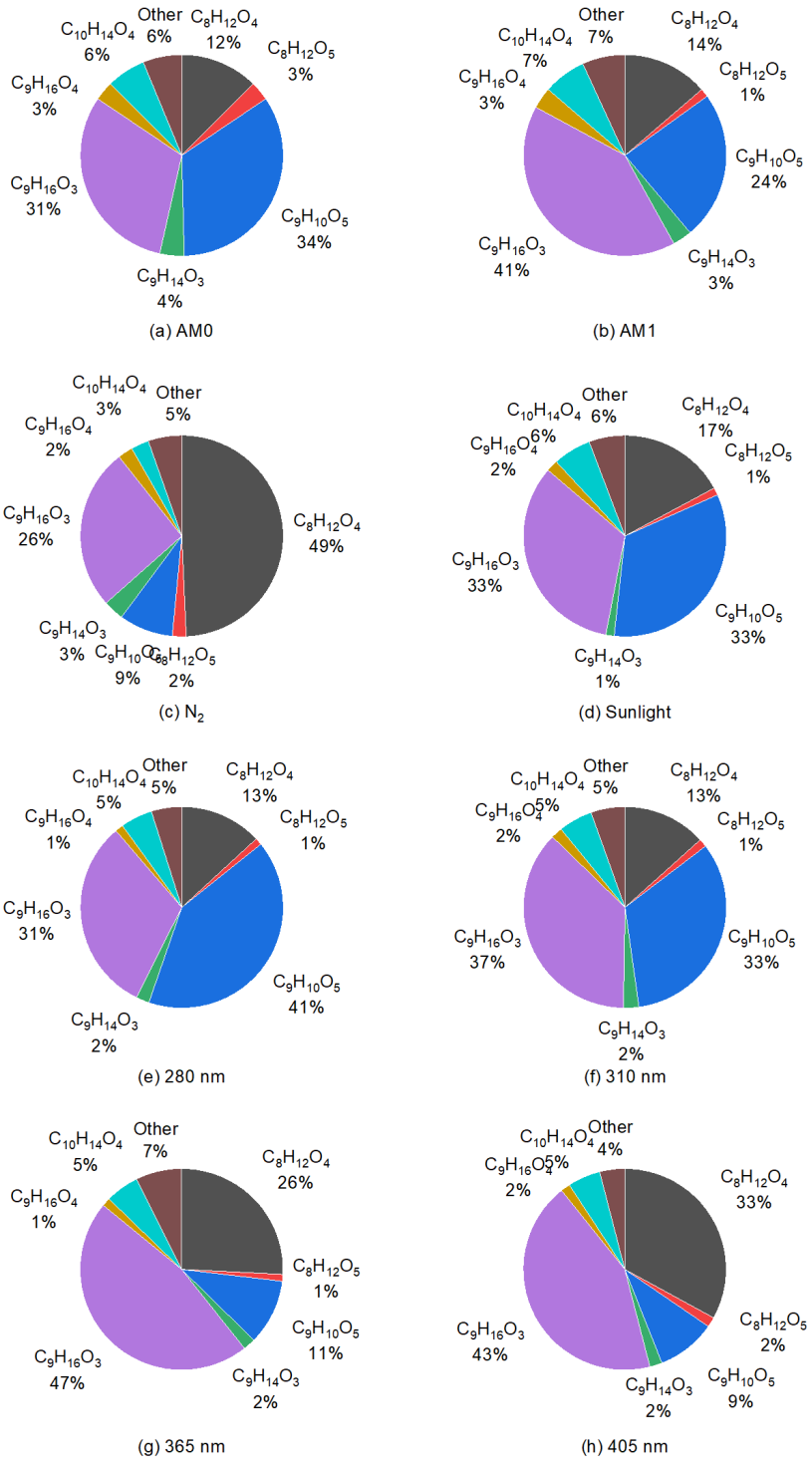


**Figure 13. Fractions of products in total liquid-phase $C_xH_yO_z$ under different irradiation conditions.**

https://doi.org/10.5194/egusphere-2025-1233
Preprint. Discussion started: 26 March 2025


In previous work by Tinel et al. 2016, the solution with 4-BBA showed the formation of $C_9H_{16}O_3$ increased by a factor of ~2.5 in the presence of air. In our study, with 4-BBA the formation of $C_9H_{16}O_3$ increased by a factor of ~11. The oxygenated $C_9$ products are promoted when $O_2$ is abundant, which is in agreement with Tinel et al. The promotion of oxygen on the formation of $C_8H_{12}O_4$ was limited. The formation of $C_8H_{12}O_4$ was significantly improved with the presence of 4-BBA, indicating that $C_8H_{12}O_4$ was a photodegradation product from NA. The following scheme shows the suggested photolysis of 4-BBA alone:

$$4BBA(C_{14}H_{10}O_3) \xrightarrow{h\nu} C_{14}H_{11}O_3$$

$$C_{14}H_{11}O_3 \xrightarrow{h\nu \leq 310\ nm, H_2O} C_6H_6 + C_8H_7O_3$$

$$C_{14}H_{11}O_3 \xrightarrow{h\nu \leq 310\ nm, H_2O} C_7H_6O + C_7H_7O_2$$

$$C_8H_7O_3 \xrightarrow{O_2, HCO_3} C_9H_{10}O_5$$

The photolysis of NA in the presence of 4-BBA could follow the following scheme:

$$4BBA(C_{14}H_{10}O_3) + C_9H_{18}O_2 \xrightarrow{h\nu} C_{14}H_{11}O_3 + C_9H_{17}O_2$$

$$C_9H_{17}O_2 \xrightarrow{O_2} C_9H_{17}O_4$$

$$C_9H_{17}O_4 \xrightarrow{RO_2} C_9H_{16}O_3 + C_9H_{18}O_3$$

$$C_9H_{17}O_4 \xrightarrow{O_2, HCO_3} C_{10}H_{14}O_4$$

$$C_9H_{16}O_3 \xrightarrow{h\nu, OH} C_9H_{14}O_3 + C_9H_{16}O_4$$

AM0 irradiation of NA solution without 4-BBA did not show any changes in the SFG signal indicating no photoreaction in the absence of 4-BBA, Fig. 1a. On the other hand, irradiating 4-BBA without NA with AM0 showed a slight decrease of the water bands at the very beginning followed by the recovery of the dark signal within one hour of irradiation, Fig. 1b. Although the changes in OH stretching modes from hydrogen-bonded interfacial water at ~3240 and 3450 $cm^{-1}$ are within the signal-to-noise, the change in the dangling OH band at ~3700 $cm^{-1}$ is noticeable. This is likely due to photodissociation of 4-BBA under UV light. Indeed, the results of the mass spectroscopy in the gas phase, blue bars in Fig. 12, confirm the dissociation of 4-BBA, after irradiation with AM0, and the emission of benzene and benzaldehyde in the absence of NA. A key question that arises is why the aromatic band at 3070 $cm^{-1}$ is absent in the SFG spectrum (Fig. 1b) after irradiation, despite its presence when irradiating the mixture in the presence of NA (Fig. 2b).

https://doi.org/10.5194/egusphere-2025-1233
Preprint. Discussion started: 26 March 2025


The photolysis process can break chemical bonds within the molecule and rearrange the atoms, resulting in the formation of new compounds. The specific conditions and reactions involved in the photolysis of 4-benzoylbenzoic acid may vary depending on factors such as the intensity and wavelength of the light, the presence of sensitizers or catalysts, and the reaction environment. The photolysis of 4-BBA acid can involve multiple reaction pathways depending on the experimental conditions and the nature of the light source. Benzene and benzaldehyde may form upon photolysis of 4-BBA through two possible reaction pathways: 1) Decarboxylation, where the carboxyl group (-COOH) is lost as carbon dioxide ($CO_2$), resulting in the formation of benzene and a carboxylic acid radical. The carboxylic acid radical can undergo further reactions, such as hydrogen abstraction or rearrangements, potentially leading to the formation of benzaldehyde. 2) Photoreduction, where in the presence of a suitable reducing agent (NA in our case), the photogenerated carboxylic acid radical can undergo reduction reactions. If NA is present in the reaction mixture, it could potentially act as a hydrogen donor or a radical scavenger. It could react with the photogenerated carboxylic acid radical, accepting a hydrogen atom and undergoing oxidation itself in the process. This reaction could lead to the formation of benzaldehyde as a primary product, along with other side products. Benzene can also be formed through subsequent reactions, such as further reduction or rearrangement of the intermediate products. The first pathway applies to the SFG experiment without NA, Fig. 1b, while the second pathway additionally applies to the SFG experiments in the presence of NA and 4-BBA, e.g. in Fig. 2b.

The appearance of the aromatic band in Fig. 2b but not in Fig. 1b after AM0 irradiation can be attributed to the properties of benzaldehyde. Benzaldehyde ($C_6H_5CHO$) is an aromatic aldehyde, consisting of both a benzene ring and an aldehyde functional group (-CHO). While it has a polar aldehyde group, the nonpolar nature of the benzene ring dominates, resulting in low solubility in water but a high affinity for organic compounds. Due to its predominantly nonpolar structure, benzaldehyde lacks the hydrophilic-hydrophobic balance required to function as a surfactant. Although its polar functional group may allow for weak interactions at the water surface, these interactions are not strong enough to significantly reduce surface tension or exhibit notable surface activity. As a result, benzaldehyde does not appear in Fig. 1b. Surface activity or surfactant properties are typically associated with amphiphilic molecules, which have both hydrophilic and hydrophobic regions. These molecules can accumulate at interfaces and reduce the surface tension of the system. This behavior arises from the orientation of surfactant molecules at the air-water interface, with their hydrophilic portions interacting with water and their hydrophobic portions interacting with nonpolar regions. On the other hand, in the presence of NA, and due to the high affinity, benzaldehyde appears at the surface and could contribute to the SFG signal as can be seen in Fig. 2b.

https://doi.org/10.5194/egusphere-2025-1233
Preprint. Discussion started: 26 March 2025


Although, the aromatic band of benzaldehyde was not detected in the absence of NA, the impact of its presence as a photoproduct appeared as a reduction in the dangling OH band after 30 min of AM0 irradiation, green curve Fig. 1b. The observed decrease in the dangling OH band intensity in the SFG spectrum upon the emergence of benzaldehyde into water is indicative of the alteration of the hydrogen bonding environment at the water surface due to the interaction between the benzaldehyde photoproduct and water molecules. Benzaldehyde, being molecule with a polar carbonyl group (-CHO), can either interact directly with the dangling OH at the surface or form hydrogen bonds with water molecules through the oxygen atom of the aldehyde group. This interaction between benzaldehyde and water can compete with the hydrogen bonding of water molecules to the dangling OH groups at the water surface. As a result, the formation of benzaldehyde leads to a reduction in the availability of free hydroxide ions causing a decrease in the intensity of the dangling OH peak observed in the SFG spectrum after 30 min of irradiation.

One possible explanation for the increase after the decrease in the dangling OH band observed in the SFG spectrum after the formation of benzaldehyde is that initially, upon the formation of benzaldehyde, its presence disrupts the hydrogen bonding network of water molecules at the water surface as described above. There are two scenarios for the afterword increase of the dangling OH signal. First, as the concentration of benzaldehyde increases beyond a certain threshold, a reverse effect may occur, e.g. benzaldehyde molecules self-aggregate or form clusters at the water surface due to their nonpolar aromatic moiety. This clustering or aggregation can create local environments that are more favorable for hydrogen bonding with water molecules leading to an increase in the intensity of the dangling OH band in the SFG spectrum. The second scenario involves the evaporation of benzaldehyde from the water surface due to its volatility. Benzaldehyde has a relatively low boiling point of around 179-180 ˚C and a significant vapor pressure, which means it can readily transition from a liquid to a gas phase at room temperature. The second scenario is the more likely to occur as is proven by the detection of benzaldehyde in the gas phase in the mass spectrometry results.

In the presence of NA, benzaldehyde and NA can interact due to their chemical properties. Benzaldehyde, with an aromatic ring and aldehyde group (-CHO), and NA, with a carboxylic acid group (-COOH), can engage in acid-base reactions. NA, a weak acid, can donate a proton, while benzaldehyde can accept it, potentially forming a conjugate acid. Additionally, they may undergo other reactions like condensation, esterification, or oxidation, depending on the conditions and presence of catalysts.

https://doi.org/10.5194/egusphere-2025-1233
Preprint. Discussion started: 26 March 2025


## 5 Conclusions

This study focuses on the correlation between the photochemical products at the surface and bulk regions. We spotlighted the complex contribution of solar power distribution, pH, salinity and surface photoproducts on the reaction mechanism. We chose nonanoic acid, as surfactant, and 4-BBA, as a photosensitizer, and compared our combined surface-bulk study to the bulk study by Tinel et al., 2016. The SFG technique allowed us to detect and confirm the partition of the non-surface-active compounds to the organic surface layer where it can induce radical reactions leading to the formation of a variety of compounds. Under the environmental conditions applied in this work, the 4-BBA was found to be acting as a source of photoproducts in addition to its expected role as a photosensitizer for the NA. The photolysis of the 4-BBA is more active when exposed to shorter wavelengths of the UV portion of the light spectrum. Benzaldehyde, formed by the photolysis of 4-BBA, plays a vital role in the photosensitized chemistry of NA at the surface.

The spectral power distribution of the day light significantly affects the photoreaction. This indicates the importance of considering the geographical position, atmospheric conditions, and the time of day and year in the modeling parametrizations. The shorter wavelength and/or higher intensity has stronger effect. The change in pH changes the concentration of partially dissociated fatty acids at the surface and influences the photo reaction rate and pathways. Preliminary results also showed that the salinity accelerates the photoreaction rate. We attributed this effect to the increase in the concentration of the 4-BBA at the air-water interface caused by the bulk dissolved salts. Further investigation of the mechanism under salty conditions is necessary to be addressed in future work. Finally, dissolved oxygen develops multiple pathways of the interactions. In nature, these processes are even more complex due to the presence of a large variety of fatty acids at the SML which enrich more organic photosensitizers at the surface. These findings apply to all water surfaces, e.g. at ocean, rivers, lakes and even cloud droplets.

https://doi.org/10.5194/egusphere-2025-1233
Preprint. Discussion started: 26 March 2025


## Author contribution

All authors have made significant contributions to this research. AA proposed the research idea, conducted the literature review, designed and built the custom solar simulator, and conceived and designed the experiments. AA led the SFG and MS experiments, performed data analysis and interpretation, and wrote and compiled the manuscript. DG conducted the SFG experiments alongside AA, contributed to the SFG data analysis, and provided critical revisions to the manuscript. YG performed the MS experiments, analyzed and interpreted the MS data in collaboration with AA, drafted the MS-related sections, and revised the MS content of the manuscript. BB supervised the SFG experiments, discussed the results with AA and DG, and reviewed the SFG-related sections. HS supervised the MS experiments, discussed the results with AA and YG, and revised the MS sections. JL contributed to the chemistry aspects of the experiments, assisted with methodology development and data collection, and participated in manuscript revisions. MF supported the estimation and validation of the solar simulator output and characteristics and assisted in final manuscript preparation.

## Acknowledgements

AA gratefully acknowledges the support of the German Research Foundation (DFG, AB 604/3-1). Special thanks are extended to Ottmar Möhler for hosting AA in his group at KIT during the finalization of the manuscript following the conclusion of the DFG project. The authors thank Olga Dombrowski for assistance with sample preparations in the chemistry lab at KIT and Thomas Leisner for hosting the first author at IMKAAF-KIT during the DFG project period. DG and BB thank the DFG for funding CRC 1459 Intelligent Matter – Project-ID 433682494. The authors acknowledge the assistance of ChatGPT in refining the abstract, author contributions, and acknowledgments text for improved clarity and professionalism.

## Competing interests

Some authors are members of the editorial board of journal ACP. The authors declare that there are no conflicts of interest regarding the publication of this paper. No financial, personal, or professional relationships influenced the research or its outcomes.

## Financial support

This research has been supported by the Deutsche Forschungsgemeinschaft (grant no. AB 604/3-1).

https://doi.org/10.5194/egusphere-2025-1233
Preprint. Discussion started: 26 March 2025


## Supplementary information

Supplementary information related to this manuscript, including additional figures, tables, and experimental procedures, is provided to support and enhance the understanding of the study. These materials offer further insight into the methods and results discussed in the main text, ensuring a comprehensive overview of the research.

## Ethical approval

This article does not involve any studies or experiments conducted on human participants or animals by any of the authors.

https://doi.org/10.5194/egusphere-2025-1233
Preprint. Discussion started: 26 March 2025


# References

Alpert, P. A., Ciuraru, R., Rossignol, S., Passananti, M., Tinel, L., Perrier, S., Dupart, Y., Steimer, S. S., Ammann, M., Donaldson, D. J., and George, C.: Fatty Acid Surfactant Photochemistry Results in New Particle Formation, Sci. Rep., 7, https://doi.org/10.1038/s41598-017-12601-2, 2017.

Backus, E. H. G., Bonn, D., Cantin, S., Roke, S., and Bonn, M.: Laser-Heating-Induced Displacement of Surfactants on the Water Surface, J. Phys. Chem. B, 116, 2703–2712, https://doi.org/10.1021/jp2074545, 2012.

Badban, S., Hyde, A. E., and Phan, C. M.: Hydrophilicity of Nonanoic Acid and Its Conjugate Base at the Air/Water Interface, ACS Omega, 2, 5565–5573, https://doi.org/10.1021/acsomega.7b00960, 2017.

Bernard, F., Ciuraru, R., Boréave, A., and George, C.: Photosensitized Formation of Secondary Organic Aerosols above the Air/Water Interface, Environ. Sci. Technol., 50, 8678–8686, https://doi.org/10.1021/acs.est.6b03520, 2016.

Boucher, O.: Atmospheric Aerosols, in: Atmospheric Aerosols: Properties and Climate Impacts, edited by: Boucher, O., Springer Netherlands, Dordrecht, 9–24, https://doi.org/10.1007/978-94-017-9649-1_2, 2015.

Brüggemann, M., Hayeck, N., and George, C.: Interfacial photochemistry at the ocean surface is a global source of organic vapors and aerosols, Nat. Commun., 9, 2101, https://doi.org/10.1038/s41467-018-04528-7, 2018.

Carlson, D. J.: Dissolved organic materials in surface microlayers: Temporal and spatial variability and relation to sea state, Limnol. Oceanogr., 28, 415–431, https://doi.org/10.4319/lo.1983.28.3.0415, 1983.

Carlson, D. J. and Mayer, L. M.: Enrichment of dissolved phenolic material in the surface microlayer of coastal waters, Nature, 286, 482–483, https://doi.org/10.1038/286482a0, 1980.

Carpenter, L. J. and Nightingale, P. D.: Chemistry and Release of Gases from the Surface Ocean, Chem. Rev., 115, 4015–4034, https://doi.org/10.1021/cr5007123, 2015.

Ciuraru, R., Fine, L., van Pinxteren, M., D'Anna, B., Herrmann, H., and George, C.: Photosensitized production of functionalized and unsaturated organic compounds at the air-sea interface, Sci. Rep., 5, 12741, https://doi.org/10.1038/srep12741, 2015.

Covington, A. K. and Whitfield, M.: Recommendations for the determination of pH in sea water and estuarine waters, Pure Appl. Chem., 60, 865–870, https://doi.org/doi:10.1351/pac198860060865, 1988.

Dickson, A. G.: The measurement of sea water pH, Mar. Chem., 44, 131–142, https://doi.org/10.1016/0304-4203(93)90198-W, 1993.

Doughty, B., Yin, P. C., and Ma, Y. Z.: Adsorption, Ordering, and Local Environments of Surfactant-Encapsulated Polyoxometalate Ions Probed at the Air-Water Interface, Langmuir, 32, 8116–8122, https://doi.org/10.1021/acs.langmuir.6b01643, 2016.

Photochemical Air Quality Modeling: https://www.epa.gov/scram/photochemical-air-quality-modeling.

Feng, R.-J., Li, X., Zhang, Z., Lu, Z., and Guo, Y.: Spectral assignment and orientational analysis in a vibrational sum frequency generation study of DPPC monolayers at the air/water interface, J. Chem. Phys., 145, 244707, https://doi.org/10.1063/1.4972564, 2016.

https://doi.org/10.5194/egusphere-2025-1233
Preprint. Discussion started: 26 March 2025


Gantt, B. and Meskhidze, N.: The physical and chemical characteristics of marine primary organic aerosol: a review, Atmos. Chem. Phys., 13, 3979–3996, https://doi.org/10.5194/acp-13-3979-2013, 2013.

García Rey, N., Weißenborn, E., Schulze-Zachau, F., Gochev, G., and Braunschweig, B.: Quantifying Double-Layer Potentials at Liquid–Gas Interfaces from Vibrational Sum-Frequency Generation, J. Phys. Chem. C, 123, 1279–1286, https://doi.org/10.1021/acs.jpcc.8b10097, 2019.

Gautam, K. S., Schwab, A. D., Dhinojwala, A., Zhang, D., Dougal, S. M., and Yeganeh, M. S.: Molecular Structure of Polystyrene at Air/Polymer and Solid/Polymer Interfaces, Phys. Rev. Lett., 85, 3854–3857, https://doi.org/10.1103/PhysRevLett.85.3854, 2000.

Ghosh, A., Campen, R. K., Sovago, M., and Bonn, M.: Structure and dynamics of interfacial water in model lung surfactants, Faraday Discuss., 141, 145–159, https://doi.org/10.1039/b805858j, 2009.

Hardt, M., Honnigfort, C., Carrascosa-Tejedor, J., Braun, M. G., Winnall, S., Glikman, D., Gutfreund, P., Campbell, R. A., and Braunschweig, B.: Photoresponsive arylazopyrazole surfactant/PDADMAC mixtures: reversible control of bulk and interfacial properties, Nanoscale, 16, 9975–9984, https://doi.org/10.1039/D3NR05414D, 2024.

Henry, M. C., Yang, Y. J., Pizzolatto, R. L., and Messmer, M. C.: Competitive adsorption of 2,4,7,9-tetramethyl-5-decyn-4,7-diol and linear alkane surfactants at the air/water interface, Langmuir, 19, 2592–2598, https://doi.org/10.1021/la026812l, 2003.

Jiang, L. Q., Carter, B. R., Feely, R. A., Lauvset, S. K., and Olsen, A.: Surface ocean pH and buffer capacity: past, present and future, Sci. Rep., 9, 18624, https://doi.org/10.1038/s41598-019-55039-4, 2019.

Karimova, N., Alija, O., Mora García, S. L., Grassian, V. H., Gerber, R. B., and Navea, J. G.: pH Dependence of the speciation and optical properties of 4-benzoylbenzoic acid, Phys. Chem. Chem. Phys., 25, 17306–17319, https://doi.org/10.1039/D3CP01520C, 2023.

Liss, P. S. and Duce, R. A.: The Sea Surface and Global Change, Cambridge University Press, 2005.

Lu, R., Gan, W., Wu, B., Zhang, Z., Guo, Y., and Wang, H.: C−H Stretching Vibrations of Methyl, Methylene and Methine Groups at the Vapor/Alcohol (n = 1−8) Interfaces, J. Phys. Chem. B, 109, 14118–14129, https://doi.org/10.1021/jp051565q, 2005.

Luo, M., Wauer, N. A., Angle, K. J., Dommer, A. C., Song, M., Nowak, C. M., Amaro, R. E., and Grassian, V. H.: Insights into the behavior of nonanoic acid and its conjugate base at the air/water interface through a combined experimental and theoretical approach, Chem. Sci., 11, 10647–10656, https://doi.org/10.1039/D0SC02354J, 2020.

MacPhail, R. A., Strauss, H. L., Snyder, R. G., and Elliger, C. A.: Carbon-hydrogen stretching modes and the structure of n-alkyl chains. 2. Long, all-trans chains, J. Phys. Chem., 88, 334–341, https://doi.org/10.1021/j150647a002, 1984.

Marion, G. M., Millero, F. J., Camões, M. F., Spitzer, P., Feistel, R., and Chen, C. T. A.: pH of seawater, Mar. Chem., 126, 89–96, https://doi.org/10.1016/j.marchem.2011.04.002, 2011.

Meerkötter, R. and Vázquez-Navarro, M.: Earth's Radiation Budget: The Driver for Weather and Climate, in: Atmospheric Physics: Background – Methods – Trends, edited by: Schumann, U., Springer Berlin Heidelberg, Berlin, Heidelberg, 55–67, https://doi.org/10.1007/978-3-642-30183-4_4, 2012.

Millero, F. J., Feistel, R., Wright, D. G., and McDougall, T. J.: The composition of Standard Seawater and the

https://doi.org/10.5194/egusphere-2025-1233
Preprint. Discussion started: 26 March 2025


definition of the Reference-Composition Salinity Scale, Deep Sea Res. Part I Oceanogr. Res. Pap., 55, 50–72, https://doi.org/10.1016/j.dsr.2007.10.001, 2008.

Miranda, P. B. and Shen, Y. R.: Liquid interfaces: A study by sum-frequency vibrational spectroscopy, J. Phys. Chem. B, 103, 3292–3307, https://doi.org/10.1021/jp9843757, 1999.

Mmereki, B. T. and Donaldson, D. J.: Laser induced fluorescence of pyrene at an organic coated air–water interface, Phys. Chem. Chem. Phys., 4, 4186–4191, https://doi.org/10.1039/b204754c, 2002.

Mora Garcia, S. L., Pandit, S., Navea, J. G., and Grassian, V. H.: Nitrous Acid (HONO) Formation from the Irradiation of Aqueous Nitrate Solutions in the Presence of Marine Chromophoric Dissolved Organic Matter: Comparison to Other Organic Photosensitizers, ACS Earth Sp. Chem., 5, 3056–3064, https://doi.org/10.1021/acsearthspacechem.1c00292, 2021.

Morgan, J. J.: Aquatic Chemistry-Chemical Equilibria and Rates in Natural Waters, USA: JOHN WILEY, 1995.

Nihonyanagi, S., Mondal, J. A., Yamaguchi, S., and Tahara, T.: Structure and dynamics of interfacial water studied by heterodyne-detected vibrational sum-frequency generation, Annu Rev Phys Chem, 64, 579–603, https://doi.org/10.1146/annurev-physchem-040412-110138, 2013.

Ouafo-Leumbe, M. R., Galy-Lacaux, C., Liousse, C., Pont, V., Akpo, A., Doumbia, T., Gardrat, E., Zouiten, C., Sigha-Nkamdjou, L., and Ekodeck, G. E.: Chemical composition and sources of atmospheric aerosols at Djougou (Benin), Meteorol. Atmos. Phys., 130, 591–609, https://doi.org/10.1007/s00703-017-0538-5, 2018.

Rao, Y., Li, X., Lei, X. G., Jockusch, S., George, M. W., Turro, N. J., and Eisenthal, K. B.: Observations of Interfacial Population and Organization of Surfactants with Sum Frequency Generation and Surface Tension, J. Phys. Chem. C, 115, 12064–12067, https://doi.org/10.1021/jp201799z, 2011.

Rosen, M. J. and Kunjappu, J. T.: Surfactants and interfacial phenomena, John Wiley & Sons, 2012.

Schultz, M. J., Baldelli, S., Schnitzer, C., and Simonelli, D.: Aqueous Solution/Air Interfaces Probed with Sum Frequency Generation Spectroscopy, J. Phys. Chem. B, 106, 5313–5324, https://doi.org/10.1021/jp014466v, 2002.

Sellegri, K., O'Dowd, C. D., Yoon, Y. J., Jennings, S. G., and de Leeuw, G.: Surfactants and submicron sea spray generation, J. Geophys. Res., 111, https://doi.org/10.1029/2005jd006658, 2006.

Shen, Y. R.: Surface Properties Probed by Second-Harmonic and Sum-Frequency Generation, Nature, 337, 519–525, https://doi.org/10.1038/337519a0, 1989.

Shultz, M. J., Schnitzer, C., Simonelli, D., and Baldelli, S.: Sum frequency generation spectroscopy of the aqueous interface: ionic and soluble molecular solutions, Int. Rev. Phys. Chem., 19, 123–153, https://doi.org/10.1080/014423500229882, 2000.

Snyder, R. G., Strauss, H. L., and Elliger, C. A.: Carbon-hydrogen stretching modes and the structure of n-alkyl chains. 1. Long, disordered chains, J. Phys. Chem., 86, 5145–5150, https://doi.org/10.1021/j100223a018, 1982.

Sovago, M., Campen, R. K., Wurpel, G. W. H., Müller, M., Bakker, H. J., and Bonn, M.: Vibrational Response of Hydrogen-Bonded Interfacial Water is Dominated by Intramolecular Coupling, Phys. Rev. Lett., 100, 173901, https://doi.org/10.1103/PhysRevLett.100.173901, 2008.

https://doi.org/10.5194/egusphere-2025-1233
Preprint. Discussion started: 26 March 2025


Tinel, L., Rossignol, S., Bianco, A., Passananti, M., Perrier, S., Wang, X., Brigante, M., Donaldson, D. J., and George, C.: Mechanistic Insights on the Photosensitized Chemistry of a Fatty Acid at the Air/Water Interface, Environ. Sci. Technol., 50, 11041–11048, https://doi.org/10.1021/acs.est.6b03165, 2016.

Truong, V. N. T., Wang, X. M., Dang, L. X., and Miller, J. D.: Interfacial Water Features at Air-Water Interfaces as Influenced by Charged Surfactants, J. Phys. Chem. B, 123, 2397–2404, https://doi.org/10.1021/acs.jpcb.9b01246, 2019.

Varga, I., Keszthelyi, T., Meszaros, R., Hakkel, O., and Gilanyi, T.: Observation of a liquid-gas phase transition in monolayers of alkyltrimethylammonium alkyl sulfates adsorbed at the air/water interface, J. Phys. Chem. B, 109, 872–878, https://doi.org/10.1021/jp048006o, 2005.

Wilson, T. W., Ladino, L. A., Alpert, P. A., Breckels, M. N., Brooks, I. M., Browse, J., Burrows, S. M., Carslaw, K. S., Huffman, J. A., Judd, C., Kilthau, W. P., Mason, R. H., McFiggans, G., Miller, L. A., Najera, J. J., Polishchuk, E., Rae, S., Schiller, C. L., Si, M., Temprado, J. V, Whale, T. F., Wong, J. P. S., Wurl, O., Yakobi-Hancock, J. D., Abbatt, J. P. D., Aller, J. Y., Bertram, A. K., Knopf, D. A., and Murray, B. J.: A marine biogenic source of atmospheric ice-nucleating particles, Nature, 525, 234-+, https://doi.org/10.1038/nature14986, 2015.

Xing, J., Zheng, S., Li, S., Huang, L., Wang, X., Kelly, J. T., Wang, S., Liu, C., Jang, C., Zhu, Y., Zhang, J., Bian, J., Liu, T.-Y., and Hao, J.: Mimicking atmospheric photochemical modeling with a deep neural network, Atmos. Res., 265, 105919, https://doi.org/10.1016/j.atmosres.2021.105919, 2022.

Zhang, D., Gutow, J., and Eisenthal, K. B.: Vibrational-spectra, orientations, and phase-transitions in long-chain amphiphiles at the air-water-interface - probing the head and tail groups by sum-frequency generation, J. Phys. Chem., 98, 13729–13734, https://doi.org/10.1021/j100102a045, 1994.